SSRG International Journal of Electrical and Electronics Engineering
ISSN: 2348-8379/ https://doi.org/10.14445/23488379/IJEEE-V13I4P108

Volume 13 Issue 4, 105-118, April 2026

Original Article

SMC Control for EMF Induced in Rotor Circuit of DFIG-Based Wind Energy Conversion System During Voltage Dips

A.Ravi Shankar[1], T.R.Jyothsna[2]

[1,2]*Department of Electrical Engineering, Andhra University, Visakhapatnam, Andhra Pradesh, India*

[1]*Corresponding Author : shankar.alluri@gmail.com*

Received: 16 January 2026 Revised: 26 February 2026 Accepted: 25 March 2026 Published: 30 April 2026

Abstract *- Variable-speed operation and partial-scale power converter capabilities are the primary reasons for the growing popularity of Wind Energy Conversion Systems (WECS) that are based on Doubly-Fed Induction Generators (DFIG). These systems are both cost-effective and efficient. However, the rotor windings are subject to substantial Electromotive Forces (EMF) when the grid voltage decreases, which can lead to excessive rotor currents, converter saturation, and the potential for grid disconnection. The conventional mitigation solutions, such as crowbar circuits and PI-based controllers, either limit the controllability of the system or lack the resilience necessary to withstand large shocks. The Sliding Mode Control (SMC) technique is proposed in this study for the rotor-side converter to modulate rotor currents and reduce induced electromagnetic fields during symmetrical and asymmetrical voltage fluctuations. Compliance with the control law is verified by testing the Low-Voltage Ride-Through (LVRT) grid code requirements, which incorporates a boundary layer to reduce chattering and features a boundary layer. This ensures robust monitoring of current references. In comparison to conventional controllers, the suggested method is shown to reduce rotor current overshoot dramatically, preserve DC-link stability, and offer fast reactive power assistance. These findings were derived from simulations carried out in MATLAB/Simulink. The results indicate that the proposed SMC is both practical and effective in enhancing the fault ride-through capability of DFIG-based WECS.*

Keywords *- Doubly-Fed Induction Generator, Wind Energy Conversion System, Sliding Mode Control, Voltage Dip, Low-Voltage Ride-Through, Rotor-Side Converter.*

1. Introduction

The global demand for sustainable electricity and stringent environmental regulations are the primary factors driving the rapid expansion of wind energy as a renewable resource. The Doubly-Fed Induction Generator (DFIG) is the most prevalent architecture among the numerous generator technologies utilized in large-scale Wind Energy Conversion Systems (WECS). Its popularity is attributed to the use of partially rated back-to-back converters (typically 25–30% of machine capacity), independent control of active and reactive power, and variable-speed operation capabilities, which ensure high efficiency and cost-effectiveness in comparison to fully rated converter systems [1, 2].

In spite of these benefits, DFIG-based WECS encounter substantial obstacles during grid disturbances, notably voltage fluctuations caused by defects or network imbalances. The rotor circuit experiences substantial Electromotive Forces (EMF) as a result of the abrupt decrease in stator voltage, which can result in overcurrents that surpass the rated capacity of the Rotor-Side Converter (RSC). If left unchecked, this could result in converter saturation, loss of synchronization, and potential disconnection from the grid, which could compromise the reliability of both the grid and the system.

In order to adhere to contemporary grid regulations, particularly those that pertain to Low-Voltage Ride-Through (LVRT), it is imperative to implement robust control strategies that restrict rotor currents, mitigate induced EMF, and facilitate reactive power injection during voltage sags. The controllability of the system is sacrificed during faults, resulting in reactive power absorption rather than injection, as traditional solutions such as crowbar circuits safeguard the converter hardware. In the same vein, conventional Proportional-Integral (PI) controllers, despite their simplicity and widespread use, exhibit parameter sensitivity and a decline in performance during severe voltage fluctuations [3]. Advanced controls, such as Model Predictive Control (MPC) and fuzzy or adaptive schemes, provide enhanced dynamics; however, they also impose a significant computational burden, additional complexity, and extensive tuning requirements. At the same time, while Sliding Mode Control (SMC) has

exhibited robustness to parameter uncertainties and strong disturbance rejection, current implementations frequently fail to fully meet grid-code LVRT standards, reduce chattering, and ensure seamless reactive power injection [4].

2. Literature Review

In order to enhance the LVRT capacity of DFIG-based WECS, a variety of methods have been proposed. Using crowbar circuits, which are designed to redirect fault currents away from the RSC, is the solution that is considered to be the most traditional. Crowbars, on the other hand, inhibit converter control during activation, which results in the DFIG absorbing reactive power rather than providing assistance to the grid [5]. DC-link choppers and series dynamic resistors are two examples of alternative techniques that may prevent overvoltage and safeguard converter components. However, these solutions come at a higher cost and are more complicated.

From a control standpoint, PI-based rotor current controllers are used extensively in commercial converters because of the ease with which they may be implemented. PI controllers, on the other hand, are very sensitive to changes in parameters and disturbances in the grid, which results in a decline in performance when the dips are particularly severe [6]. Control methods that are resilient and nonlinear have been investigated to address these limitations. Model predictive control (MPC) is encumbered by a substantial quantity of computational labor, despite its ability to provide rapid dynamics. Controllers that are fuzzy and adaptive provide versatility, but they need a significant amount of tweaking [7]. SMC has recently attracted attention for DFIG systems due to its invariance characteristic and immunity to external disturbances and parameter uncertainties. This is because SMC can control the system inherently [8]. It has been shown in previous research that SMC is capable of successfully regulating rotor currents in the presence of grid disturbances and improving the performance of LVRT. Despite this, there are still obstacles to overcome in terms of simplification of implementation, reduction of chattering, and integration of reactive power injection needs that are imposed by grid regulations [9, 10].

Because several methods for the protection and management of DFIGs have been offered, the literature that was studied highlighted the fact that each of these systems has significant limitations. Crowbars and choppers are examples of hardware-based approaches that have a tendency to degrade the controllability of the system and increase overall expenses [11]. While sophisticated techniques such as MPC entail considerable computing loads, conventional PI controllers lack the resilience necessary to withstand quick transients and parameter fluctuations. This makes it difficult for these controllers to be used in real time [12]. In addition, the SMC approaches that are now in use often fail to completely align with the grid-code-based LVRT criteria. This is especially true concerning the injection of reactive current when fault events occur [13]. These shortcomings highlight a significant research gap, which is the requirement for a control strategy that is not only reliable and computationally efficient, but also grid-compliant. This control strategy should be able to suppress rotor overcurrents, mitigate induced electromotive forces, and maintain stable operation under both symmetrical and asymmetrical voltage dips [14].

2.1. Research Gap

The literature reveals a critical gap: current methods either rely on control methods that lack robustness or grid conformance, or on costly or complex hardware-based protections that reduce system flexibility. In particular, there is an urgent requirement for a control strategy that:

- Effectively mitigates rotor current surges and induced EMF during both symmetrical and asymmetrical voltage declines.
- Rapidly injects reactive power to meet LVRT criteria without the need for additional hardware.
- Reduces control chattering to facilitate practical real-time implementation.
- Ensures consistent operation in the face of unpredictable grid disturbances and fluctuating wind velocities.

2.1.1. Problem Statement and Motivation

It is imperative to address this disparity to improve the fault ride-through capabilities of DFIG-based WECS, which will allow for the integration of a greater amount of wind power without compromising grid stability. The urgent need to improve DFIG-based WECS fault ride-through capabilities to meet changing grid codes motivated this study. With more wind power in contemporary power systems, even short-term disruptions might compromise grid stability if huge wind farms disconnect during faults. A control solution that eliminates dependency on additional hardware, while ensuring strong robustness against uncertainties, would reduce cost, enhance reliability, and make wind power integration more sustainable. Sliding Mode Control is a compelling candidate due to its disturbance rejection capability, invariance to parameter uncertainties, and ease of implementation in digital controllers. To suppress fault-induced EMF, modulate rotor currents, and simultaneously provide reactive power support to the grid, it is feasible to customize SMC for the rotor-side converter of DFIG. This combination is a significant source of motivation for the current investigation.

2.1.2. Novelty of the Work

The primary objective of the proposed study is to enhance the fault-tolerant performance of grid-connected Doubly-Fed Induction Generators. The primary objective of the research is to develop a dependable Sliding Mode Control method for the rotor-side converter that can effectively mitigate the EMF generated by defects during voltage fluctuations. The control

technique is much more robust since it incorporates grid-code-compliant LVRT capabilities, which allow reactive current injection during symmetrical and asymmetrical faults without an extra piece of hardware. Asymptotic convergence of rotor current dynamics under constrained disturbances is guaranteed by a thorough stability study based on Lyapunov theory. The design takes a boundary layer technique to improve the real-time applicability of SMC by addressing actual implementation issues and dramatically reducing chattering. A comprehensive evaluation of the efficacy of the proposed technique is conducted using MATLAB/Simulink simulations. These simulations are benchmarked against traditional PI control and uncontrolled scenarios spread over various operating conditions.

3. System Description

In the wind energy conversion system that was investigated, three primary subsystems make up the system: (i) the aerodynamic turbine model, (ii) the drive train and mechanical dynamics, and (iii) the electrical generator along with its accompanying power electronic converters. Figure 1 shows the DFIG-based WECS schematic. Through a back-to-back voltage source converter that is comprised of the RSC and the Grid Side Converter (GSC), the stator is directly tied to the grid, whilst the rotor is connected to the grid through a back-to-back mechanism [15]. The RSC is primarily responsible for governing the rotor currents and serving as a decoupled control mechanism for both active and reactive power, while the GSC is responsible for maintaining the DC-link voltage and ensuring grid stability. Subsequent subsections furnish additional information regarding the system.

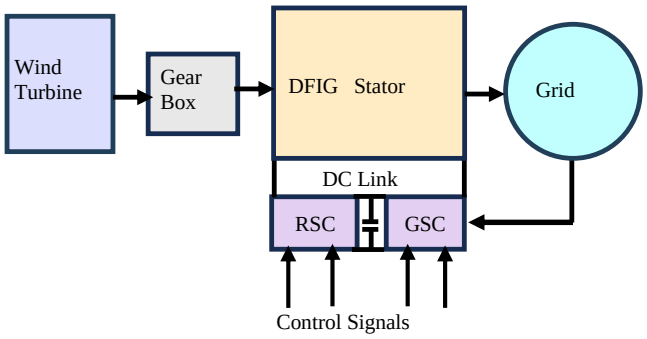

Fig. 1 DFIG-based WECS schematic diagram

3.1. Aerodynamic Model of Wind Turbine

It is possible to represent the power that is gathered from the wind as:

$$P_w = \frac{1}{2}\rho A C_p(\lambda,\beta) v_w^3 \qquad (1)$$

Where ρ is the air density, $A=\pi R^2$ is the swept area of the turbine blades with radius R, v_w is the wind speed, and $C_p(\lambda, \beta)$ is the power coefficient, which is a nonlinear function of the blade pitch angle and the tip-speed ratio, are all variables in this context [16]. The ratio of tip speed to total speed is

$$\lambda = \frac{\omega_t R}{v_w} \qquad (2)$$

where the turbine's angular speed is represented by ω_t in rad/s, the shaft's aerodynamic torque can be determined by the following formula:

$$T_m = \frac{P_w}{\omega_t} \qquad (3)$$

Through the use of a gearbox, this torque is what powers the DFIG rotor.

3.2. Drive Train and Mechanical Dynamics

The wind turbine is effectively connected to the generator by employing a transmission with a gear ratio of N_g. For this reason, the turbine speed is directly proportional to the high-speed shaft angular velocity, denoted as ω_r.

$$\omega_r = N_g\, \omega_t \qquad (4)$$

It is possible to get a description of the mechanical dynamics of the shaft using.

$$J\frac{d\omega_r}{dt} = T_m - T_e - B\omega_r \qquad (5)$$

J is the generator-turbine moment of inertia, B is the viscous friction coefficient, and Te is the DFIG's electrical torque.

3.3. Electrical Model of DFIG

In the DFIG, a wound-rotor induction machine, the stator windings are directly connected to the grid and the rotor windings to the back-to-back converter via slip rings [17]. The dynamic model of the machine is given in the synchronous dq-reference frame. These formulas calculate stator voltage:

$$v_{qs} = R_s i_{qs} + \frac{d\lambda_{qs}}{dt} + \omega_s \lambda_{ds} \qquad (7)$$

The equations for the rotor voltage are presented similarly.

$$v_{dr} = R_r i_{dr} + \frac{d\lambda_{dr}}{dt} - (\omega_s - \omega_r)\lambda_{qr} \qquad (8)$$

$$v_{qr} = R_r i_{qr} + \frac{d\lambda_{qr}}{dt} + (\omega_s - \omega_r)\lambda_{dr} \qquad (9)$$

where v_{ds}, v_{qs}, and v_{dr}, v_{qr} denote the voltages of the stator and rotor, i_{ds}, i_{qs}, and i_{dr}, i_{qr} denote the currents in those

respective components, R_s, R_r represent the resistances in that component, $ö_s$ denotes the speed in synchronous rotation, and $ö_r$ denotes the speed in rotor rotation in electrical radians. The flux linkages are stated as follows:

$$\lambda_{ds} = L_s i_{ds} + L_m i_{dr} \quad (10)$$

$$\lambda_{qs} = L_s i_{qs} + L_m i_{qr} \quad (11)$$

$$\lambda_{dr} = L_r i_{dr} + L_m i_{ds} \quad (12)$$

$$\lambda_{qr} = L_r i_{qr} + L_m i_{qs} \quad (13)$$

The stator and rotor self-inductances are denoted by *L*s and *L*r, respectively, while the mutual inductance is denoted by L_m. Specifically, the electromagnetic torque may be expressed as

$$T_e = \frac{3}{2}\frac{P}{2}\left(\lambda_{ds} i_{qs} - \lambda_{qs} i_{ds}\right) \quad (14)$$

P represents the total number $_{of}$ poles that the machine has.

3.4. Induced EMF During Voltage Dips

An abrupt change in stator flux results from a drop in grid voltage because of the stator voltage's rapid drop. Stator magnetic coupling changes create an EMF in the rotor windings. The induced EMF may be roughly estimated if the stator voltage drops from V_s to α V_s (0<α<1).

$$e_r = \frac{L_m}{L_s}(1-\alpha)V_s \quad (15)$$

The converter's ratings may be exceeded by the huge transient rotor currents caused by the produced EMF. In order to suppress these currents and guarantee steady and safe operation, it is vital to manage the RSC effectively.

The constant flux linkage theorem states that the air-gap flux stays intact when a DFIG experiences a voltage drop. The steady-state natural component may be found by equating the stator flux in steady state before the dip with the algebraic sum of the symmetrical components at the dip. This component decays with the stator circuit's time constant. The rotor conductors' EMF comes from their relative motion with the symmetrical stator flux components.

$$\psi_s^s(t_0^-) = \psi_s^s(t_0^+) \quad (16)$$

Stator flux in terms of symmetrical components.

$$\psi_s^s = \psi_{s1}^s + \psi_{s2}^s + \Psi_{sn}^s \quad (17)$$

$$\psi_r^s = \psi_{r1}^s + \psi_{r2}^s + \Psi_{rn}^s \quad (18)$$

The rotor voltage expressed in terms of symmetrical components can be written as

$$e_r = e_{r1} + e_{r2} + e_{rn} \quad (19)$$

$$e_{r_1}^s + e_{r_2}^s + e_{r_n}^s = |\psi_{s1}^s| e^{js\omega_s t}.j.s\omega_s - |\psi_{s2}^s| e^{-j(2-s).\omega_s t}.j.(2-s).\omega_s - |\psi_{sn}^s| e^{-j\omega_m t}.j.\omega_m \quad (20)$$

Where

$$\psi_S^S = \frac{V_S}{j\omega_S} \quad \psi_{S1}^S = \frac{V_{S1}}{j\omega_S} \quad and \ \psi_{S2}^S = \frac{V_{S2}}{-j\omega_S}$$

The expression for the EMF induced in the rotor circuit for symmetrical and asymmetrical faults can be written as

For 3-phase stator voltage dip

$$e_r = \left(\frac{Lm}{Ls}\right).V_{pre}.\{(1-K).e^{js\omega_s t}.s - (1-s).K.e^{-j\omega_m t}.e^{-t/\tau}\} \quad (21)$$

For single-phase stator dip (t_0=0)

$$e_r = \left(\frac{Lm}{Ls}\right).V_{pre}.\{\left(1-\frac{K}{3}\right).e^{js\omega_s t}.s - (2-s).K/3.e^{-j.(2-s).\omega_s t}\} \quad (22)$$

For single-phase stator dip (t_0=T/4)

$$e_r = \left(\frac{Lm}{Ls}\right).V_{pre}.\{\left(1-\frac{K}{3}\right).e^{js\omega_s t}.s + (2-s).\frac{K}{3}.e^{-j.(2-s).\omega_s t} - j.\left(\frac{2}{3}\right).K.s.e^{-j\omega_m t}.e^{-t/\tau}\} \quad (23)$$

For phase-to-phase dip (t_0=0)

$$e_r = \left(\frac{Lm}{Ls}\right).V_{pre}.\left\{\left(1-\frac{K}{2}\right).e^{js\omega_s t}.s + (2-s).\frac{K}{2}.e^{-j.(2-s).\omega_s t} - (1-s).e^{-j\omega_m t}.e^{-t/\tau}\right\} \quad (24)$$

For phase-to-phase dip (t_0=T/4)

$$e_r = \left(\frac{Lm}{Ls}\right).V_{pre}.\{\left(1-\frac{K}{2}\right).e^{js\omega_s t}.s - j(2-s).\frac{K}{2}.e^{-j.(2-s).\omega_s t}\} \quad (25)$$

4. Design of Sliding Mode Control

During grid disruptions, the Rotor-Side Converter (RSC) in DFIGs is crucial. Excessive currents are produced when the voltage dips because the rotor is subjected to significant EMFs caused by the abrupt change in stator flux [18, 19]. Therefore, the goals of the suggested controller are as follows: (i) Keeping Rotor currents within safe bounds; (ii) reducing the impact of induced EMF during grid failures; and (iii) making sure that LVRT complies with grid code requirements. This is accomplished by using a sliding mode control-based robust

nonlinear control strategy, which offers excellent disturbance rejection capabilities and invariance to system uncertainties. Figure 2 shows the block diagram of the control architecture for DFIG-based WECS. Where RG- Reference Generation, CT-Coordinate Transformation, AW Pi-Anti Windup PI, VOC- Voltage Oriented Control.

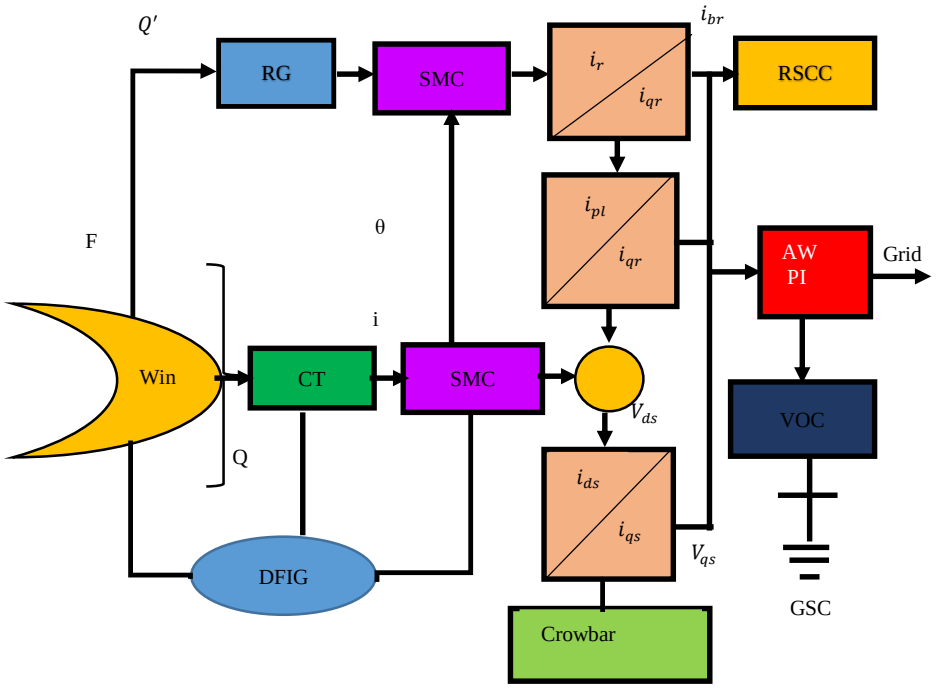

Fig. 2 A DFIG-based WECS Control Architecture Block Diagram

4.1. Rotor Current Model

Reduced-order dynamic model of rotor current in synchronous dq-reference frame:

$$\dot{i}_r = A\, i_r + B\, u + d(t) \tag{26}$$

Ai_r - Rotor current vector, Bu-RSC control input vector, and grid voltage dips and modeling errors are represented by d(t). A definition of the system matrices is

$$A = \begin{bmatrix} -a & \omega_{sl} \\ -\omega_{sl} & -a \end{bmatrix}, B = bI_2 \tag{27}$$

with unchanging values

$$a = \frac{R_r}{\sigma L_r}, b = \frac{1}{\sigma L_r}, \tag{28}$$

In this equation, the rotor resistance is denoted by R_r, the rotor inductance is denoted by L_r, the leakage factor is represented by σ, and the slip angular frequency is denoted $\omega_{sl}=\omega_s-\omega_r$. The fundamental dynamics of the rotor current under perturbations are encapsulated in this formulation.

4.2. Sliding Surface Definition

The tracking error between actual and reference rotor currents determines the sliding surface design. Defining error:

$$s_i = i_r^{ref} - i_r \tag{29}$$

The reference rotor current vector, denoted as $i_r^{ref,}$ is calculated from the active and reactive power needs, also known as LVRT requirements. The sliding surface is selected as a means to guarantee that the error dynamics will converge.

$$S = \dot{s}_i + \Lambda s_i \tag{30}$$

where the positive definite matrix $\Lambda=diag(\lambda_d, \lambda_q)$ controls the rate of convergence in the components along the *d*- and *q*-axis. As the system trajectory approaches this surface, the rotor current error dynamics stabilize first-order.

4.3. Equivalent Control Law

$\dot{S}=0$ is met in the absence of disturbances by use of the analogous control. By replacing the present dynamics with (30), the corresponding control input can be obtained as

$$u_{eq} = B^{-1}\left(\dot{i}_r^{ref} + \Lambda \dot{s}_i - A i_r\right) \tag{31}$$

Under perfect circumstances, this term ensures steady-state tracking by canceling out the system's nominal dynamics.

4.4. Discontinuous (Switching) Control

As the analogous control cannot eliminate external disturbances, such as produced EMF, a discontinuous control term is introduced to protect system trajectories from straying off the sliding surface:

$$u_{sw} = -K \cdot sgn(S) \quad (32)$$

K=diag(k_d,k_q) is a positive gain diagonal matrix. This switching control resists confined shocks and uncertainty.

Consequently, the whole sliding mode control rule is as follows:

$$u = u_{eq} + u_{sw} \quad (33)$$

This brings together the robust switching component and the dynamics-canceling equivalent component.

4.5. Boundary Layer to Reduce Chattering

Due to the discontinuous signum function in equation (32), traditional SMC suffers from high-frequency oscillation, often referred to as chattering. To reduce the impact of this, a saturation function is used in place of the signum function in a boundary layer approach:

$$u = u_{eq} - K \cdot sat\left(\frac{S}{\phi}\right) \quad (34)$$

where ϕ is the thickness of the boundary layer, this adjustment keeps the control signal resilient to disturbances within the specified layer while also smoothing it out.

4.6. Stability Analysis

For ensuring stability, the Lyapunov candidate function should be considered.

$$V = \frac{1}{2} S^{\top} S \quad (35)$$

A time derivative is obtained by taking the

$$\dot{V} = S^{\top} \dot{S} \quad (36)$$

Therefore, the derivative meets the condition by replacing the control rule and taking into consideration bounded disturbances.

$$\dot{V} \leq -\eta \parallel S \parallel \quad (37)$$

For a constant η greater than zero. In spite of the existence of voltage dips and parameter uncertainties, this inequality provides evidence that the system trajectories converge asymptotically to the sliding surface and continue to be stable.

5. Results and Discussion

To validate the SMC approach submitted for consideration, MATLAB/Simulink was used to simulate a 2 MW, 690 V, 50 Hz DFIG-based wind energy conversion system. In the synchronous dq-reference frame, the DFIG and wind turbine were modeled using aerodynamic and drive-train dynamics.

For DC-link voltage maintenance, the GSC employed a typical Voltage-Oriented Control (VOC), while the SMC algorithm controlled the rotor-side converter RSC. Simulate parameters: Wind turbine specifications: Power: 2 MW, 0 to 25 m/s wind speed, 0° to 25° pitch angle. Tip Speed Ratio (λ): 6-8°, Pitch Angle Range: 0-25°. DFIG parameters: 2MW rated power, 690 V line-to-line stator voltage, 300-500 V rotor voltage via converter, 50 Hz stator frequency.

The wind speed profile was adjusted to oscillate between 9 and 14 m/s in order to simulate real-world scenarios. Two potential failure scenarios existed for the PCC: Asymmetrical three-phase voltage decrease (Case 1): The grid voltage was reduced to 40% of its nominal value for 150 milliseconds. The second case is an asymmetrical drop in single-phase voltage, whereby one phase is lowered to 30% of its nominal value for 200 ms.

Three controllers were put into place for the purpose of comparing performance: (1) In an open-loop scenario, there is no control/ uncontrolled, (2) Traditional regulation of current based on PI, (3) Current control based on SMC proposed.

Figure 3 illustrates the relationship between the Power Coefficient (Cp) and the Tip Speed Ratio (λ) in the context of optimizing wind turbine performance. The graph demonstrates the aerodynamic efficacy of a wind turbine at different operating conditions by illustrating the relationship between the power coefficient and the tip speed ratio.

The power coefficient initially increases significantly as the tip speed ratio increases from zero, suggesting that the wind is more effectively captured. This trend continues until it reaches a peak value C_p_max ≈ 0.50 at an optimal tip speed ratio of λ_C_p_max ≈ 7.5**.** Beyond this point, the curve gradually declines, signifying reduced efficiency due to aerodynamic losses and suboptimal rotor dynamics.

This peak represents the turbine's maximum power extraction point, where the rotor speed is ideally matched to the wind speed, maximizing energy conversion. Understanding this curve is essential for designing control strategies that maintain operation near λ_C_p_max, ensuring optimal performance and energy yield in variable wind conditions.

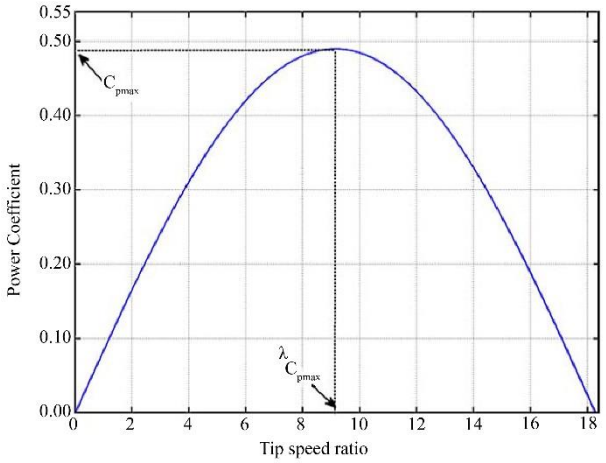

Fig. 3 Variation of Power Coefficient (Cp) with Tip Speed Ratio (λ) for Wind Turbine

Figure 4 illustrates the correlation between tip motion and Cp for the No control, PI control, and SMC control techniques. This chart compares how well various control strategies work to get the most electricity out of the wind turbine. With the highest peak Cp, the Hybrid control is more efficient at the TSR when Cp is maximal. Because of this, the MPC control's peak Cp value is somewhat smaller, but its power coefficient operating range is broader at higher TSRs. It implies that turbulent flow control captures a lower peak power coefficient and that a restricted range is unable to gather power at various TSRs, which typically results in turbid flow.

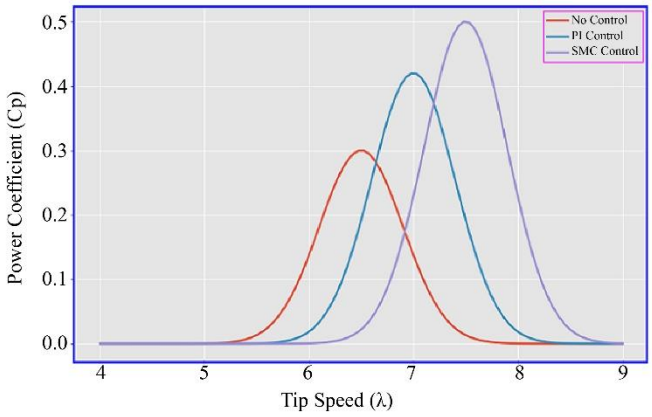

Fig. 4 Relationship between Cp and tip speed for different control

Figure 5 shows the time-varying wind speed profile for the transient analysis. The graph shows a 6s interval piecewise wind speed profile, which is often employed in wind turbine dynamic response studies under a controlled disturbance situation. In the first two seconds, the wind speed is 9 m/s, which is typical for the working circumstances. The wind speed mimics a brief dip caused by a fault or gust at 2s and then stabilizes at 5 m/s for the subsequent 2s. The control system of the turbine has difficulty in maintaining stability and power production in the face of this sudden shift. The system's recovery behavior and fault ride-through capabilities may be evaluated when the wind speed returns to 9 m/s after 4s. When it comes to systems like DFIGs, where grid compliance and operational dependability depend on keeping rotor current, DC-link voltage, and torque stable during wind variations, such profiles are crucial for assessing the resilience of control schemes.

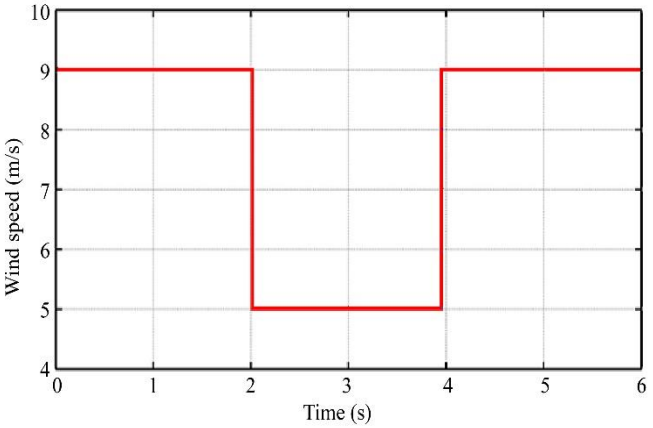

Fig. 5 Time-Varying Wind Speed Profile for Transient Analysis

Within the context of the step changes in wind speed, the usual perspective of the supply voltage is shown in Figure 6. Voltage values fluctuate between -2 and +2 per unit throughout 6 seconds, as seen in the voltage-time graph, which presents a dynamic electrical response. System events like fault injection, control switching, or load fluctuation are suggested by the discrete transitions around 2 seconds and 4 seconds in the waveform.

At first glance, the signal seems to be quite steady. However, each transition point causes a noticeable pattern shift, which indicates that the operating circumstances have changed. Graphs like this are useful for assessing how well control techniques in grid-connected systems keep voltage stable and guarantee dependable performance, since they show how the system reacts to transient disruptions and recovery phases. Figure 7 is a depiction of the normal perspective of the load voltage after correction.

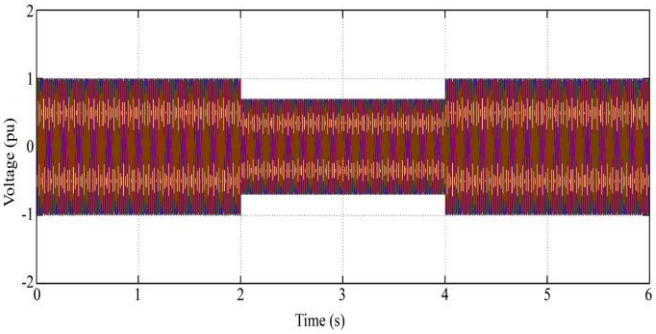

Fig. 6 Voltage as a function of the discrete variations in wind speed

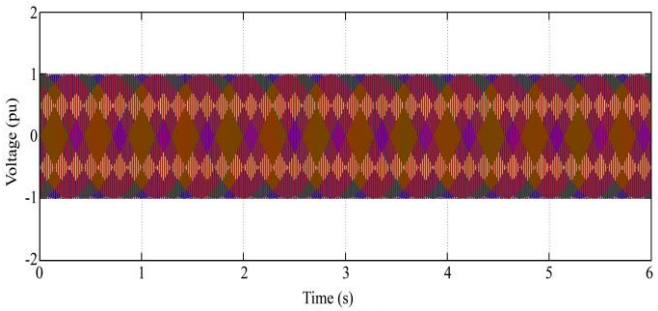

Fig. 7 Typical view of load voltage after correction

5.1. Rotor Current Response

A symmetrical three-phase dip is illustrated in Figure 8 for rotor current response. Without control, the rotor current surged to 3.5p.u., which exceeds converter safety limitations and may trip. The PI controller reduced peak current to 2.2p.u., but recovery took over 150ms. However, the recommended SMC recovered in 50ms from a 1.4p.u. rotor current overrun.

The accompanying graph shows the rotor current response under three different control schemes during a voltage dip event (from 0.05 s to 0.15 s): Uncontrolled, PI Control, and the Proposed SMC. With a peak rotor current of around 2.4p.u. and a settling time of about 0.35 seconds, the Uncontrolled technique shows poor dynamic performance. The PI Control approach outperforms this by settling in about 0.25 seconds and reducing the peak to around 1.6p.u. With a peak rotor current of just around 1.2p.u. and a settling time of only about 0.18 seconds, the Proposed SMC shows that it is better in performance. Evidence of the SMC method's efficacy in reducing spikes in rotor current and improving system stability in the face of voltage changes is shown here.

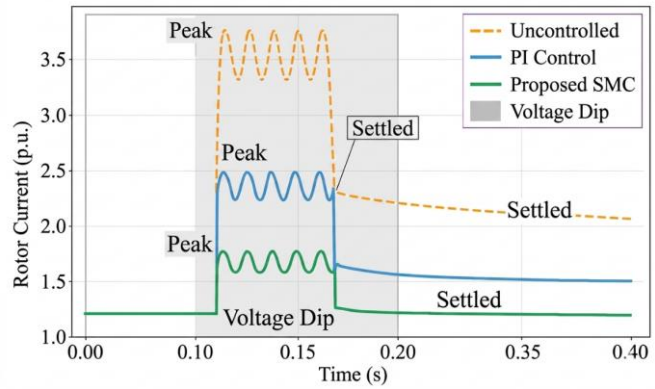

Fig. 8 Rotor current response during symmetrical three-phase voltage dip

5.2. DC-Link Voltage Stability

An essential measure of converter stability is the DC-link voltage. The failure phase was characterized by a significant overvoltage of the uncontrolled system, surpassing 1.6 p.u., as shown in Figure 9. Although recovery took longer than expected, the PI-controlled system successfully kept the deviance below 1.2 p.u. The SMC kept the DC-link voltage within 1.05 p.u. Whether the load was symmetrical or asymmetrical, so the converter could continue to operate safely, this proves that the suggested control strategy is more effective in preventing disturbances.

When a fault occurs between 0.10 and 0.25 s, the DC link voltage reacts in one of three ways, as shown in the attached graph: uncontrolled, Pf control, and the proposed sliding mode control. Poor voltage regulation is shown by the Uncontrolled method's strong oscillations throughout the fault period, which causes the DC Link Voltage to drop to around 0.65 p.u. and fluctuate dramatically. While some dips and oscillations still occur, the pf Control improves stability and keeps the voltage at 0.85 p.u. However, the DC Link Voltage stays about 1.0 p.u. The Proposed SMC performed most reliably during the fault. This proves beyond a reasonable doubt that the SMC method is better at managing faults; it guarantees stable voltage support and improves system dependability even when faced with transient disruptions.

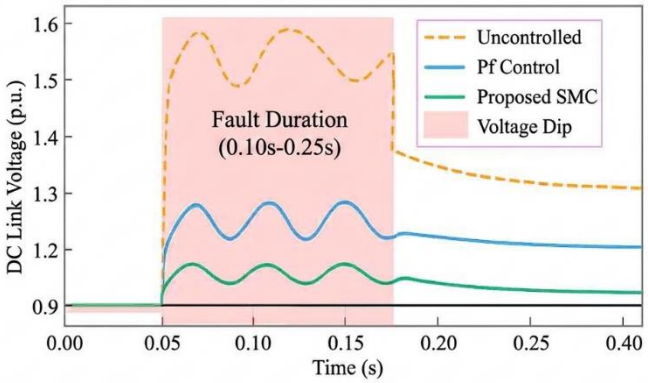

Fig. 9 DC link voltage during fault condition

5.3. Reactive Power Support and LVRT Compliance

In modern grid protocols, wind farms must stay connected during disturbances and inject reactive current proportionate to the voltage drop. PI controller support was limited and delayed. Fast reactive current injection from the SMC technique supported LVRT grid voltage recovery [20, 21]. The suggested control protects the converter and improves grid stability using this feature.

Table 1. Effect of Various Control Strategies on the reactive power response in the Event of an LVRT Failure

Time (s)	Demand (Reactive Support)	No Control (Q)	PI Control (Q)	SMC Control (Q)
0-2	0 VAR	~0 VAR	~0 VAR	~0 VAR
2-4	High reactive injection	Absorbing Q	Delayed Q rise	Fast Q injection
4-6	Recovery phase	Slow recovery	Partial support	Stable Q output

Each control strategy's response to a grid failure between 2s and 4s is summarized in Table 1. In violation of LVRT requirements, the uncontrolled /No Control system absorbs reactive power instead of injecting it.

Delays and partial assistance are provided by the PI Controller. Full compliance with grid rules is ensured by the SMC Controller's instant reaction, which involves injecting the necessary reactive current and facilitating voltage recovery.

5.4. Comparative Performance Analysis

The performance of various control schemes is summarized in Table 2, which includes both symmetrical and asymmetrical dip configurations. When compared to the conventional options that are now accessible, the technology that has been recommended provides a substantial benefit in terms of current suppression, recovery speed, voltage stability, and compliance with grid codes. Figure 10 presents a comparison of the performance of three different techniques: no control, PI control, and SMC under malfunctioning conditions.

Table 2. Comparative Performance of Control Strategies

Method	Peak Rotor Current	Recovery Time	DC-Link Overshoot	Reactive Power Support	LVRT Compliance
No Control	3.5 p.u.	>300 ms	1.6 p.u.	Poor	Fail
PI Controller	2.2 p.u.	150 ms	1.2 p.u.	Moderate	Partial
Proposed SMC	1.4 p.u.	50 ms	1.05 p.u.	Strong	Pass

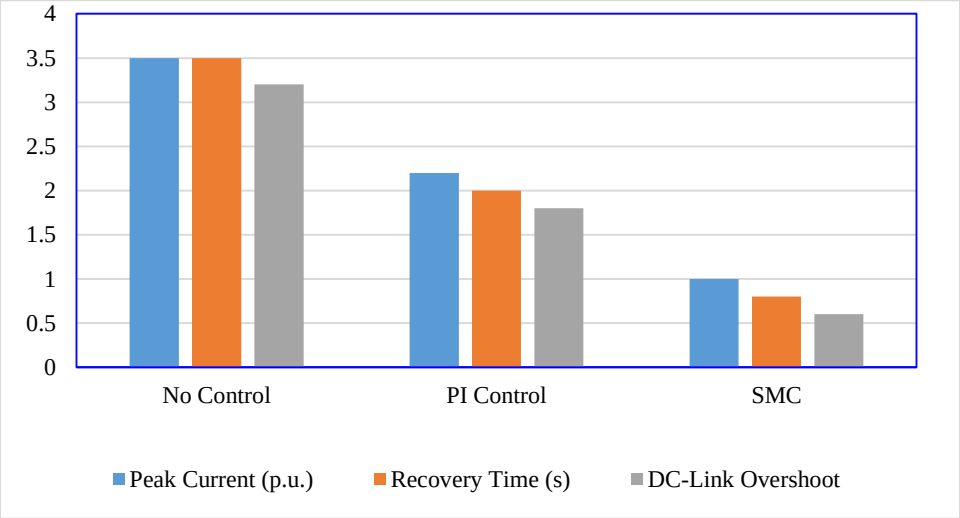

Fig. 10 Comparative Analysis of Control Strategies on Rotor Current, Recovery Time, and DC-Link Overshoot

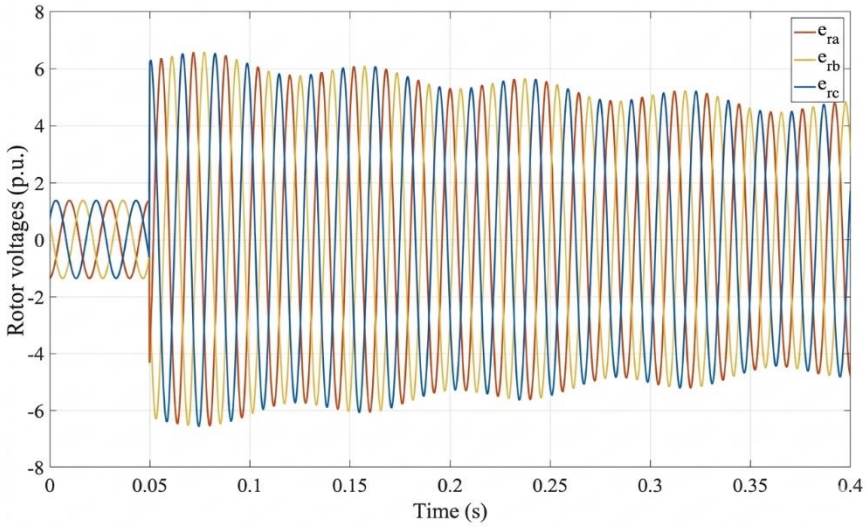

Fig. 11(a) Rotor winding EMF during stator partial voltage drops

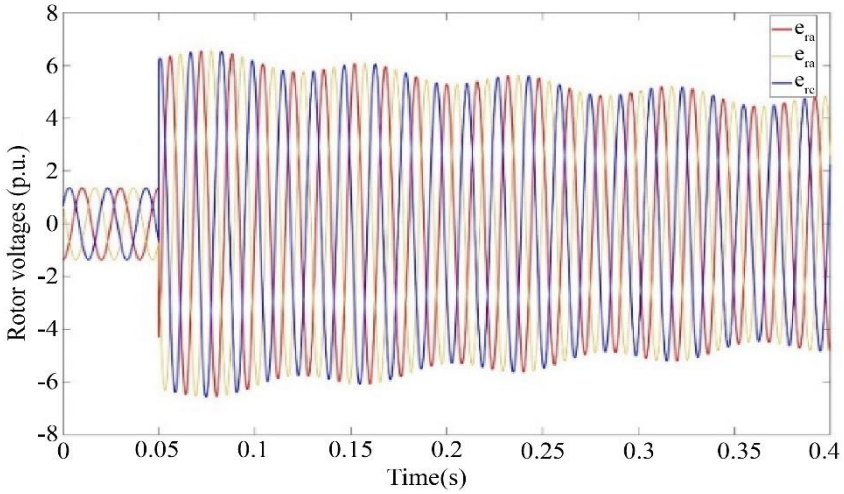

Fig. 11(b) SMC controller-induced rotor winding EMF during stator partial voltage drop

Figure 11 Rotor circuit EMF with 80% stator voltage drop with and without SMC controller.

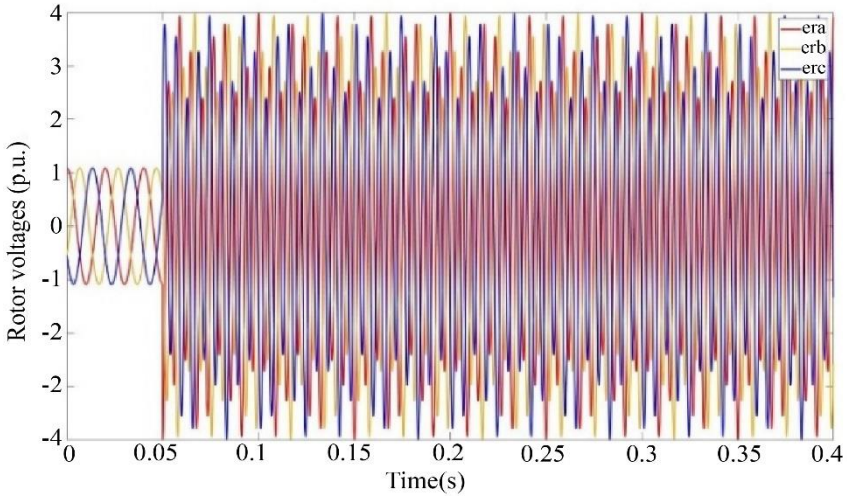

Fig. 12(a) Single-phase voltage drop at t0=0 induces rotor winding EMF.

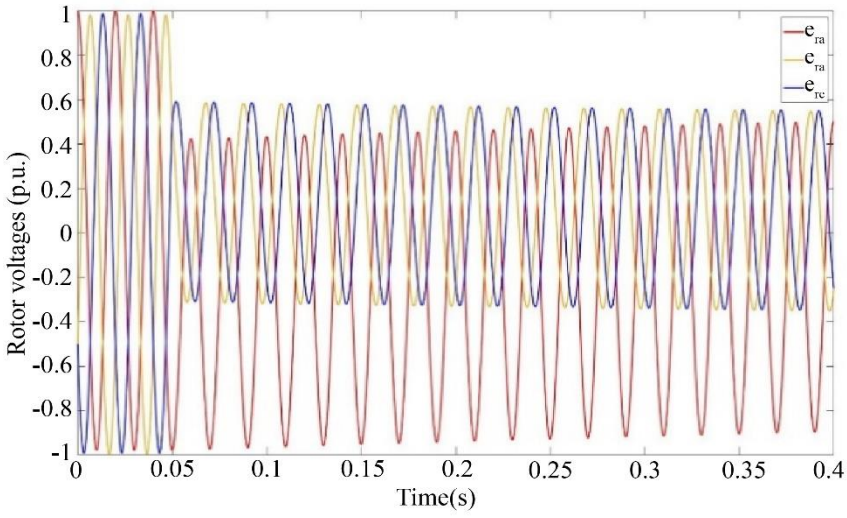

Fig. 12(b) SMC controller-induced rotor winding EMF during single voltage phase drop at t0=0.

Figure 12 Stator single-phase voltage drop at time t0=0 with and without an SMC controller, as well as the EMF created in the rotor circuit.

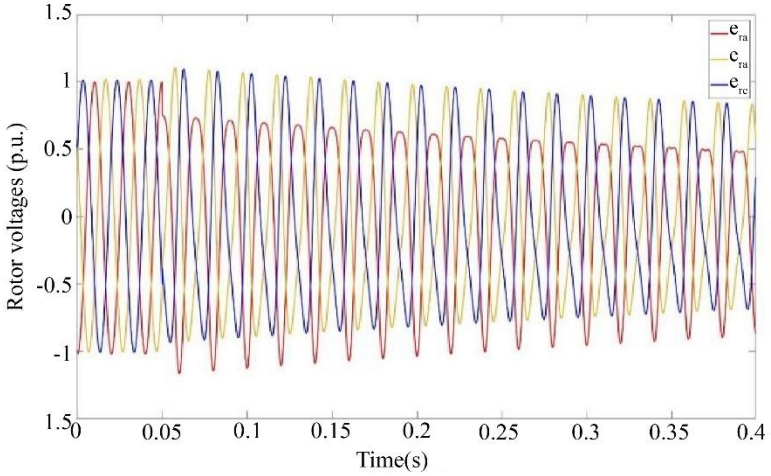

Fig. 13(a) Single -phase dip at t0=T/4 induces EMF in rotor winding.

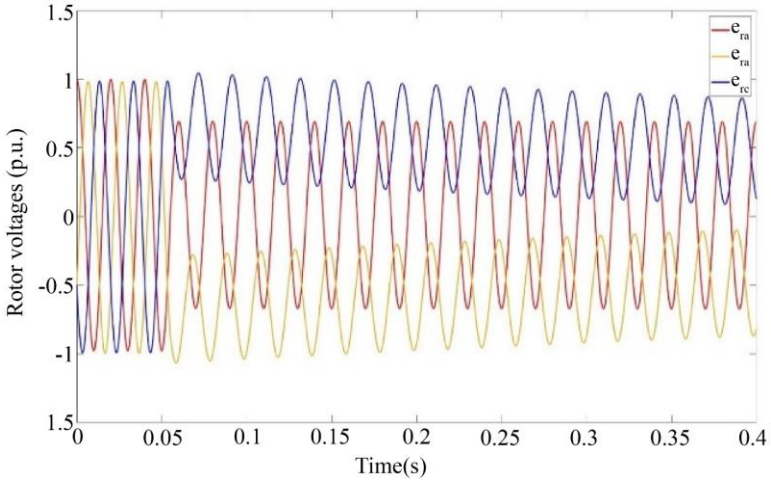

Fig. 13(b) During single-phase dip at t0=T/4, SMC controller induces EMF in rotor winding.

Figure 13 SMC controller- and non-SMC controller-induced EMF in the rotor circuit during an 80% drop in stator single-phase voltage at time t_0=T/4.

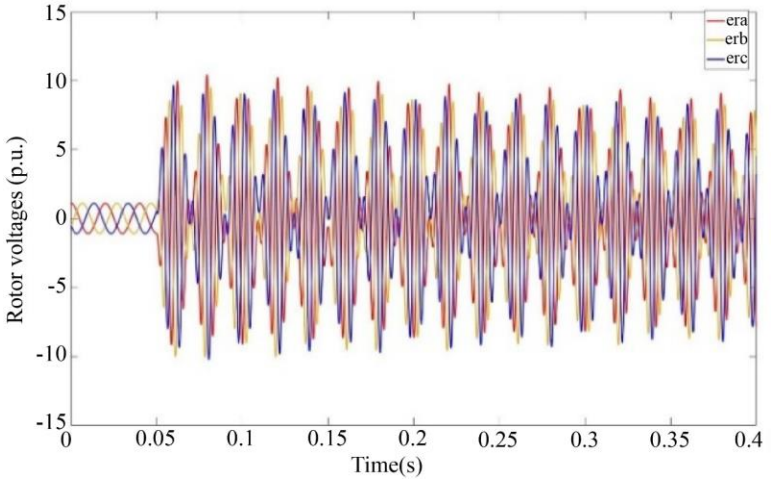

Fig. 14(a) Rotor winding EMF during phase-to-phase drop at t_0=0.

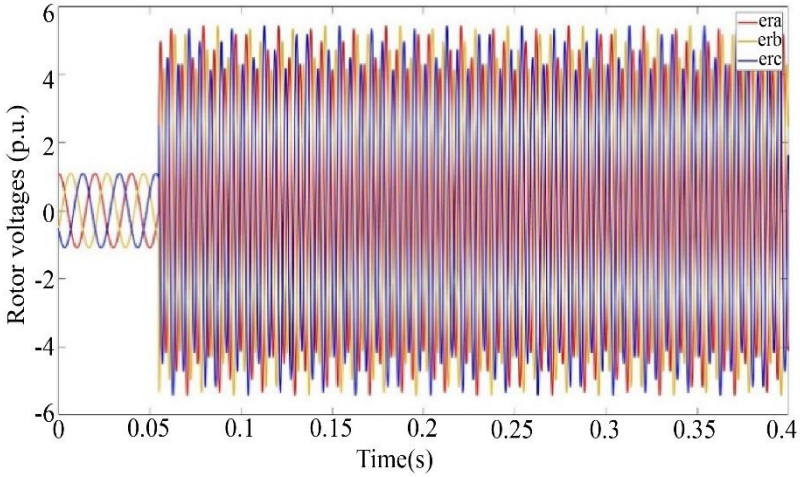

Fig. 14(b) Rotor winding EMF during phase-to-phase drop at t_0=0.

Figure 14 shows the induced EMF in the rotor circuit with and without an SMC controller during an 80% stator phase-to-phase voltage drop at instant t_0=0.

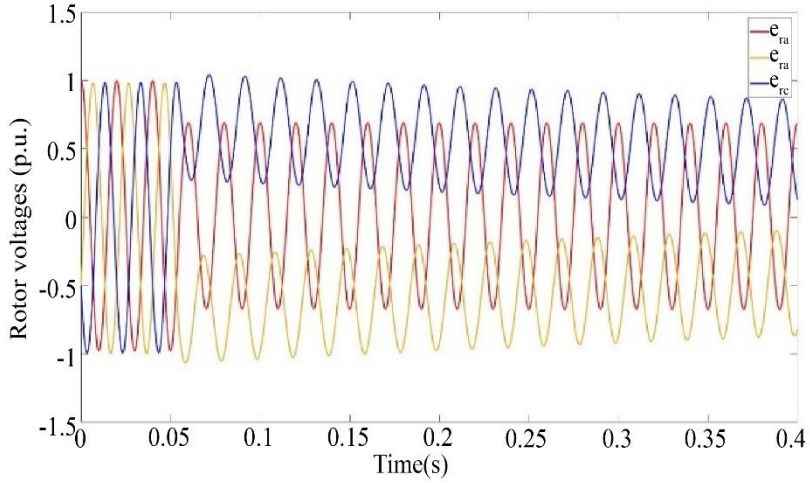

Fig. 15(a) Rotor winding EMF during phase-to-phase drop at t_0=T/4.

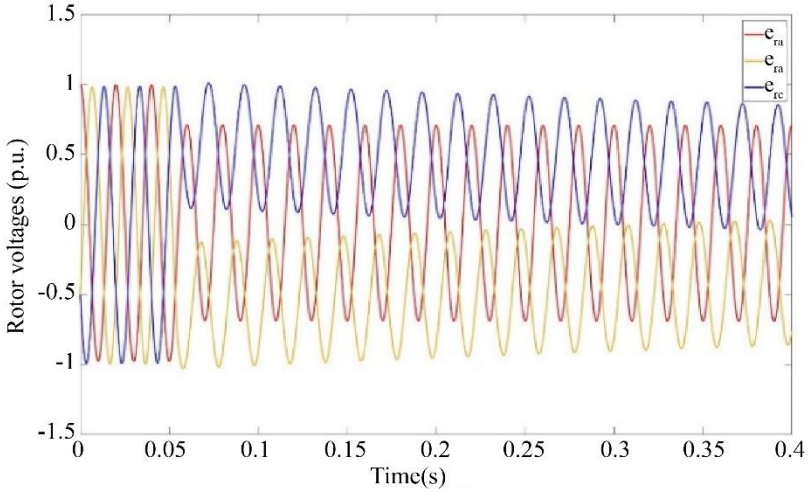

Fig. 15(b) Rotor winding EMF during phase-to-phase drop at t_0=T/4

Figure 15 shows the induced EMF in the rotor circuit with and without an SMC controller during an 80% stator phase-to-phase voltage drop at instant t_0=T/4.

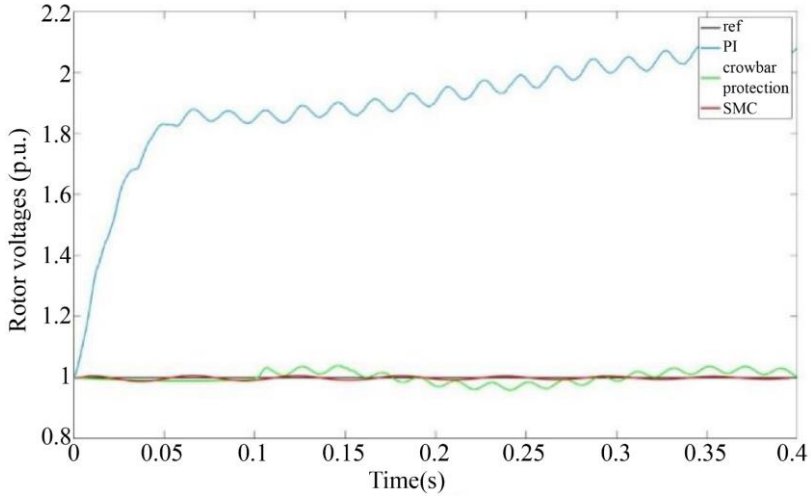

Fig. 16 Voltage drop across the capacitor

Figure 16 Capacitor voltage drop with PI controller, crowbar protection, and SMC controller (in the event of a voltage dip).

6. Discussion

The findings demonstrate that the SMC is capable of successfully mitigating induced EMF during voltage dips, hence providing steady rotor current dynamics and minimizing converter overloading when appropriate. When compared to PI control, the SMC exhibits a more rapid recovery and a greater resilience against perturbations that are inconsistent with the equilibrium. It is important to note that the suggested approach incorporates LVRT requirements by injecting reactive current without the need for external hardware. This eliminates the demand for crowbar circuits or DC choppers.

The boundary layer technique inside SMC was found to lessen chattering effects, which resulted in the control law being more appropriate for real-time implementation. This is another notable discovery. Furthermore, the Lyapunov-based design ensures stability under constrained disturbances, which assures dependable operation regardless of the wind speed or grid fault circumstances that may be present.

7. Conclusion and Future Work

This work presents an SMC method to reduce fault-induced EMF in DFIG-based wind energy conversion systems' rotor circuits during grid voltage drops. The control strategy that was presented was developed with the intention of regulating rotor currents, preventing overcurrent transients, and ensuring compliance with low-voltage ride-through regulations. Simulations showed that the SMC reduces rotor current overshoot, stabilizes DC-link voltage, and injects reactive power quickly to help the grid. These studies were carried out under both symmetrical and asymmetrical failures. In comparison to the traditional PI-based control, the suggested technique was able to produce lower peak rotor currents (1.4 p.u. against 2.2 p.u.), quicker recovery (50 ms vs 150 ms), and better LVRT compliance. All of these improvements were accomplished without the need for additional hardware such as crowbars or choppers.

On a symmetrical three-phase voltage dip, the stationary component of the stator flux produces a rotor voltage that relies on speed and decays exponentially with the stator time constant. Asymmetrical dips, such as a single-phase dip at the zero crossing or a phase-to-phase dip at 25% of the time period, have insignificant stationary flux components. As a result, the transient effect on the rotor-induced voltage is less significant compared to cases where a single-phase dip occurs at one-quarter of the time period or a phase-to-phase dip occurs at the zero crossing. In these more severe scenarios, the induced rotor voltage can reach up to five times the rated value, with a high frequency of oscillation that poses a risk of damaging the rotor-side converter. To address this, a Sliding Mode Control (SMC) strategy implemented in the rotor-side converter effectively regulates the rate of change of rotor current, mitigating both the amplitude and oscillations of the induced voltage, and keeping them within safe operational limits.

In conclusion, the SMC-based technique increases DFIG-based WECS fault ride-through capability, which secures wind energy integration into modern power systems. Future study will test Hardware-In-The-Loop (HIL), validate Real-Time Digital Simulation (RTDS), and apply the recommended technique to multi-machine wind farms.

References

[1] Ion Boldea et al., "Fractional kVA Rating PWM Converter Doubly Fed Variable Speed Electric Generator Systems: An Overview in 2020," *IEEE Access*, vol. 9, pp. 117957-117968, 2021. [CrossRef] [Google Scholar] [Publisher Link]

[2] T. Ghennam et al., "Advanced Control System of DFIG based Wind Generators for Reactive Power Production and Integration in a Wind Farm Dispatching," *Energy Conversion and Management*, vol. 105, pp. 240-250, 2015. [CrossRef] [Google Scholar] [Publisher Link]

[3] Gang Wen et al., "Dynamic Voltage and Current Assignment Strategies of Nine-Switch-Converter-Based DFIG Wind Power System for Low-Voltage Ride-Through (LVRT) Under Symmetrical Grid Voltage Dip," *IEEE Transactions on Industry Applications*, vol. 52, no. 4, pp. 3422-3434, 2016. [CrossRef] [Google Scholar] [Publisher Link]

[4] Ehsan Gatavi et al., "An Integrated Reactive Power Control Strategy for Improving Low Voltage Ride-Through Capability," *Chinese Journal of Electrical Engineering*, vol. 5, no. 4, pp. 1-14, 2019. [CrossRef] [Google Scholar] [Publisher Link]

[5] Zahra Rafiee et al., "Enhancement of the LVRT Capability for DFIG-Based Wind Farms Based on Short-Circuit Capacity," *IEEE Systems Journal*, vol. 16, no. 2, pp. 3237-3248, 2022. [CrossRef] [Google Scholar] [Publisher Link]

[6] Abdallah Fouad et al., "Enhancing Grid-Connected DFIG's LVRT Capability Using Dandelion Optimizer Based the Hybrid Fractional-Order PI and PI Controlled STATCOM," *IEEE Access*, vol. 12, pp. 120181-120197, 2024. [CrossRef] [Google Scholar] [Publisher Link]

[7] Dingdou Wen et al., "Improved Supertwisting Nonsingular Fast Terminal Sliding Mode Observer-Based Deadbeat Fault-Tolerant Predictive Control for IPMSM Demagnetization Fault," *IEEE Transactions on Power Electronics*, vol. 39, no. 10, pp. 13643-13658, 2024. [CrossRef] [Google Scholar] [Publisher Link]

[8] Ke Li et al., "Overview of Sliding Mode Control Technology for Permanent Magnet Synchronous Motor System," *IEEE Access*, vol. 12, pp. 71685-71704, 2024. [CrossRef] [Google Scholar] [Publisher Link]

[9] N. Kanagaraj et al., "Experimentation of Multi-Input Single-Output Z-Source Isolated DC–DC Converter-Fed Grid-Connected Inverter with Sliding Mode Controller," *Sustainability*, vol. 15, no. 24, pp. 1-22, 2023. [CrossRef] [Google Scholar] [Publisher Link]

[10] Yi Zhang et al., "Voltage Sag Evaluation in Power Grids Considering the Voltage Support Capabilities of Doubly-Fed Wind Farms During LVRT," *IEEE Transactions on Power Delivery*, vol. 40, no. 3, pp. 1540-1553, 2025. [CrossRef] [Google Scholar] [Publisher Link]

[11] Jinman Luo et al., "Lyapunov Based Nonlinear Model Predictive Control of Wind Power Generation System with External Disturbances," *IEEE Access*, vol. 12, pp. 5103-5116, 2024. [CrossRef] [Google Scholar] [Publisher Link]

[12] A. Ravi Shankar, and T.R. Jyothsna, "Innovative Aerodynamic and Fault Tolerant Control for VSVP Wind Turbines and DFIG Using Predictive and Sliding Mode Techniques," *Journal of Machine and Computing*, vol. 5, no. 3, pp. 1889-1904, 2025. [CrossRef] [Google Scholar] [Publisher Link]

[13] Lu Sun et al., "Analytical Model and Topology Optimization of Doubly-Fed Induction Generator," *CES Transactions on Electrical Machines and Systems*, vol. 8, no. 2, pp. 162-169, 2024. [CrossRef] [Google Scholar] [Publisher Link]

[14] Bahia Kelkoul, and Abdelmadjid Boumediene, "Stability Analysis and Study Between Classical Sliding Mode Control (SMC) and Super Twisting Algorithm (STA) for Doubly Fed Induction Generator (DFIG) Under Wind Turbine," *Energy*, vol. 214, 2021. [CrossRef] [Google Scholar] [Publisher Link]

[15] Frede Blaabjerg, Meng Chen, and Liang Huang, "Power Electronics in Wind Generation Systems," *Nature Reviews Electrical Engineering*, vol. 1, pp. 234-250, 2024. [CrossRef] [Google Scholar] [Publisher Link]

[16] S. Morteza Aghaeinezhad et al., "Individual Pitch Angle Control of a Variable Speed Wind Turbine Using Adaptive Fractional Order Non-Singular Fast Terminal Sliding Mode Control," *International Journal of Precision Engineering and Manufacturing*, vol. 22, pp. 511-522, 2021. [CrossRef] [Google Scholar] [Publisher Link]

[17] Zimin Jiang, and Yutian Liu, "Low-Voltage Ride-Through Remote Testing Method for Offshore Wind Turbines," *IEEE Transactions on Instrumentation and Measurement*, vol. 69, no. 6, pp. 2905-2913, 2020. [CrossRef] [Google Scholar] [Publisher Link]

[18] F.M. Ebrahimi, A. Khayatiyan, and E. Farjah, "A Novel Optimizing Power Control Strategy for Centralized Wind Farm Control System," *Renewable Energy*, vol. 86, pp. 399-408, 2016. [CrossRef] [Google Scholar] [Publisher Link]

[19] M. Vijayakumar, and S. Vijayan, "Photovoltaic Interfaced Three-phase Four-wire Unified Power Quality Conditioner with Extended Reference Current Generation Scheme," *Australian Journal of Electrical & Electronics Engineering*, vol. 12, no. 2, pp. 94-112, 2015. [Google Scholar] [Publisher Link]

[20] S. Tohidi et al., "Low Voltage Ride-Through of DFIG and Brushless DFIG: Similarities and Differences," *Electric Power Systems Research*, vol. 110, pp. 64-72, 2014. [CrossRef] [Google Scholar] [Publisher Link]

[21] Bibhu Prasad Ganthia, and Subrat Kumar Barik, "Fault Analysis of PI and Fuzzy-Logic-Controlled DFIG-based Grid-Connected Wind Energy Conversion System," *Journal of The Institution of Engineers (India): Series B*, vol. 103, pp. 415-437, 2022. [CrossRef] [Google Scholar] [Publisher Link]

[22] Milad Shojaee, and S. Mohsen Azizi, "Decentralized Robust Controller Design for Strongly Interconnected Generators," *IEEE Access*, vol. 11, pp. 16085-16095, 2023. [CrossRef] [Google Scholar] [Publisher Link]